CHEMISTRY OF MATERIALS

Article

pubs.acs.org/cm

High-Pressure Study of $Mn(BH_4)_2$ Reveals a Stable Polymorph with High Hydrogen Density

Nikolay A. Tumanov,[†] Elsa Roedern,[‡] Zbigniew Łodziana,[§] Dorrit B. Nielsen,[‡] Torben R. Jensen,[‡] Alexandr V. Talyzin,[∥] Radovan Černý,[⊥] Dmitry Chernyshov,[#] Vladimir Dmitriev,[#] Taras Palasyuk,[$] and Yaroslav Filinchuk*[,†]

[†]Institute of Condensed Matter and Nanosciences, Université Catholique de Louvain, Place L. Pasteur 1, 1348 Louvain-la-Neuve, Belgium

[‡]Center for Materials Crystallography, Interdisciplinary Nanoscience Center (iNANO) and Department of Chemistry, University of Aarhus, Langelandsgade 140, DK-8000 Aarhus C, Denmark

[§]INP Polish Academy of Sciences, Department of Structural Research, ul. Radzikowskiego 152, 31-342 Kraków, Poland

[∥]Department of Physics, Umeå University, Linnaeus väg 24, Umeå S-90187, Sweden

[⊥]Laboratory of Crystallography, DQMP, University of Geneva, quai Ernest-Ansermet 24, 1211 Geneva, Switzerland

[#]Swiss Norwegian Beamlines at the European Synchrotron Radiation Facility, 71 Avenue des Martyrs, 38000 Grenoble, France

[$]Institute of Physical Chemistry, Polish Academy of Sciences, Kasprzaka 44/52, 01-224 Warsaw, Poland

Supporting Information

ABSTRACT: High-pressure behavior of α-$Mn(BH_4)_2$ was studied up to 29.4 GPa in diamond anvil cells using powder X-ray diffraction combined with DFT calculations and Raman spectroscopy, and two new polymorphs were discovered. The first polymorph, δ-$Mn(BH_4)_2$, forms near 1 GPa and is isostructural to the magnesium analogue δ-$Mg(BH_4)_2$. This polymorph is stable upon decompression to ambient conditions and can also be obtained by compression of α-$Mn(BH_4)_2$ in a large-volume steel press as well as by high-energy ball milling. It shows a high volumetric density of hydrogen of 125 g H_2/L at ambient conditions. δ-$Mn(BH_4)_2$ was refined in the space group $I4_1/acd$ with the cell parameters a = 7.85245(6), c = 12.1456(2) Å, and V = 748.91(1) Å^3 at ambient conditions; it can also be described in a stable P-4n2 superstructure. Its thermal stability was studied by in situ X-ray powder diffraction and thermal analysis coupled with mass-spectroscopy. δ-$Mn(BH_4)_2$ transforms back to α-$Mn(BH_4)_2$ upon heating in the temperature range of 67−109 °C in Ar (1 bar) or H_2 (100 bar) atmosphere, and a decomposition is initiated at 130 °C with the release of hydrogen and some diborane. $Mn(BH_4)_2$ undergoes a second phase transition to δ'-$Mn(BH_4)_2$ in the pressure range of 8.6−11.8 GPa. δ'-phase is not isostructural to the second high-pressure phase of $Mg(BH_4)_2$, and its structure was determined in the $\sqrt{2}a \times c$ supercell compared to the δ-phase and refined in the space group $Fddd$ with a = 9.205(17), b = 9.321(10), c = 12.638(15) Å, and V = 1084(3) Å^3 at 11.8 GPa. Equations of state were determined for α- and δ-$Mn(BH_4)_2$.

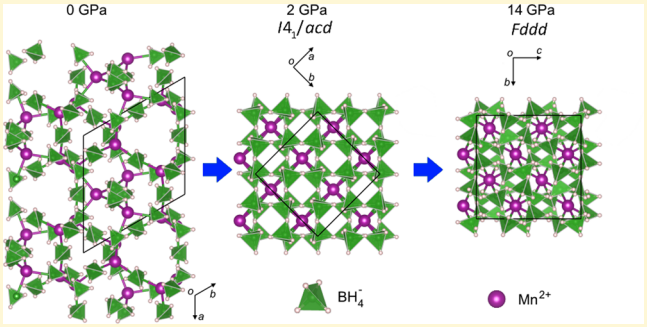

INTRODUCTION

Hydrogen economy is one of the prospective trends in the future of renewable energy, but hydrogen storage is still a limiting factor. Hydrogen storage technologies currently focus on the use of compressed gas (700 bar) for cars, but the gravimetric or volumetric hydrogen storage density is not optimal. A possible alternative may be chemically bound hydrogen in lightweight compounds. In this context, metal borohydrides have been studied intensively in recent years.[1−4] One of the problems in the practical application of metal borohydrides as hydrogen storage materials is often a too high or too low decomposition temperature.[1,2,4] Schrauzer[5] and, later, Nakamori et al.[6] showed that the stability of metal borohydrides correlates with the Pauling electronegativity of the metal (χ_p), which may be mainly defined by the complex-forming metal.[3] Manganese borohydride with χ_p = 1.55 is one of the borohydrides with a moderate temperature of decomposition (160 °C)[7,8] and could be used as a precursor for synthesis of bimetallic or trimetallic borohydrides.[9,10] The structure and properties of metal borohydrides are usually studied at ambient conditions, variable temperatures, and gas pressures up to 200 bar. Applying high hydrostatic pressure to

Received: October 22, 2015
Revised: November 27, 2015
Published: November 30, 2015

DOI: 10.1021/acs.chemmater.5b04102
Chem. Mater. 2016, 28, 274−283

the compounds not only adds an additional dimension to the phase diagram, revealing new high-pressure polymorphs of metal borohydrides,[11−20] but may also allow for the discovery of new high-pressure phases that are stable upon decompression.[18] Such compounds are not only denser than those known to form at ambient conditions but may also provide new or improved properties to a system, e.g., regarding stability, decomposition, melting temperatures, and so forth. For instance, δ-$Mg(BH_4)_2$, obtained by compression of α-$Mg(BH_4)_2$ or γ-$Mg(BH_4)_2$ to ∼1 GPa, and the pressure-collapsed amorphous $Mg(BH_4)_2$, are more stable in air[18,21] than the ambient pressure phases. The present work describes the synthesis, stability, and properties of new, dense, high-pressure polymorphs of $Mn(BH_4)_2$.

EXPERIMENTAL SECTION

Materials. α-$Mn(BH_4)_2$, used in diamond anvil cell experiments, was synthesized by two procedures. The first is via high-energy ball milling of $LiBH_4$ and $MnCl_2$ in stoichiometric amounts, producing $Mn(BH_4)_2$ with two equivalents of LiCl (sample S1).[22] The other method is based on a metathesis reaction of $MnCl_2$ and $NaBH_4$ in diethyl ether that yielded $NaMn_2(BH_4)_2{\cdot}2Et_2O$ followed by desolvation under vacuum, allowing for a chloride-free sample containing $Mn(BH_4)_2$ and only a small amount of $NaBH_4$ to be obtained (sample S2).[23]

α-$Mn(BH_4)_2$, used in steel press and high-energy ball milling experiments, was synthesized from $MnCl_2$ (anhydrous, 99.99%) and $LiBH_4$ (95%) by a metathesis reaction in anhydrous diethyl ether followed by extraction with dimethylsulfide, yielding a solvate that was desolvated at elevated temperatures (T = 110 °C) under dynamic vacuum yielding α-$Mn(BH_4)_2$ containing small amounts of $LiBH_4$ as an impurity (sample S3).

To clarify a possible influence of LiCl presence on the properties of $Mn(BH_4)_2$, we prepared the last sample by mixing α-$Mn(BH_4)_2$ (S3) and two equivalents of LiCl. The mixture was milled under argon atmosphere in an 80 mL tungsten carbide vial with 10 mm diameter balls using a Fritsch Pulverisette 6 with a ball-to-powder ratio of 1:30 at 300 rpm for 12 × 5 min with a 2 min pause in between, yielding sample S4. Table 1 summarizes the origin of samples S1−S4.

Table 1. Samples Used in High-Pressure Experiments on $Mn(BH_4)_2$

sample name	reactants/synthetic method	products, wt %
S1	$MnCl_2$ and $LiBH_4$/ball-milling	$Mn(BH_4)_2$ 50%, LiCl 50%
S2	$MnCl_2$ and $NaBH_4$/metathesis in Et_2O	$Mn(BH_4)_2$ 69%, $NaBH_4$ 31%
S3	$MnCl_2$ and $LiBH_4$/metathesis in Et_2O, extraction with dimethylsulfide	$Mn(BH_4)_2$ 90%, $LiBH_4$ 10%
S4	S3 and LiCl/ball-milling	$Mn(BH_4)_2$ 45%, LiCl 50%, $LiBH_4$ 5%

Steel Press Synthesis of δ-$Mn(BH_4)_2$. A sample of 500 mg of α-$Mn(BH_4)_2$ (S3) was loaded into a hydraulic stainless steel press with a piston of 10 mm diameter. A pressure of approximately 1.2 GPa was applied for 3 h; then, the produced pellet was removed from the press and crushed in a mortar, and the powder was reloaded and pressurized in a similar way for another 3 h. The mixture of α-$Mn(BH_4)_2$ (S4) with two equivalents of LiCl, ball milled in argon atmosphere, was pressurized using the same procedure.

Raman Spectroscopy. Raman spectra were obtained in diamond anvil cells using a Renishaw 1000 spectrometer with a 633 nm excitation laser. The pressure was calibrated using the internal ruby standard.

Thermal Analysis. The samples were studied by combined thermogravimetry (TG), differential scanning calorimetry (DSC), and mass spectrometry (MS) of the evolved gas using a PerkinElmer STA 6000 apparatus and a Hiden Analytical HPR-20 QMS sampling system. Samples of approximately 12 mg were placed in an Al crucible and heated from RT to 500 °C at a heating rate of 5 °C/min in 20 mL/min argon flow. The evolved gas was transported to the MS through heated tubing and analyzed for H_2 (m/z = 2) and B_2H_6 (m/z = 26).

In-House X-ray Powder Diffraction (XPD). Laboratory XPD was performed using a Rigaku Smart Lab X-ray diffractometer configured with a Cu X-ray source and a parallel beam multilayer mirror (Cu $K_{\alpha1}$ radiation, λ = 1.540593 Å). Data were collected at RT between 5 and 70° 2θ at 3°/min. Air-sensitive samples were mounted in 0.5 mm borosilicate glass capillaries in a glovebox and sealed by melting.

Synchrotron Radiation ex Situ X-ray Powder Diffraction (SR-XPD). High resolution SR-XPD data of δ-$Mn(BH_4)_2$, sample S3, mounted in a 0.5 mm borosilicate glass capillary, was obtained at BMI11 at the Diamond Light Source, Didcot, UK, λ = 0.825770(4) Å, with a multianalyzing crystal (MAC) detector with 5 MAC arms with 45 MAC channels between 0−150° 2θ. Three data sets with 10 min collection times were each summed, and the data was rebinned with a step size of 0.010° 2θ.

Synchrotron Radiation X-ray Powder Diffraction in Diamond Anvil Cells (DACs). Hydrostatic pressure in the X-ray powder diffraction experiments was created in a ETH-type[24] diamond anvil cell (flat culets with a diameter of 0.5 mm, a stainless steel gasket, a starting thickness of 0.200 mm preindented to 0.060 mm, and a hole diameter of 0.25 mm). The pressure was estimated from the shift in the R_1-band of a ruby calibrant (±0.05 GPa).[25,26] Because $Mn(BH_4)_2$ may be sensitive to oxygen and moisture, the fine powder of $Mn(BH_4)_2$ (samples S1 and S2) was loaded into DAC in a glovebox with a high-purity argon atmosphere. No pressure-transmitting medium was used, but quasi-hydrostatic conditions were achieved, as we found from a small broadening of ruby fluorescence lines[25,27] and the splitting of R_1-R_2 lines.[28]

High-resolution X-ray powder diffraction experiments were carried out using a synchrotron radiation source at BM1A station at the Swiss-Norwegian Beamlines at ESRF (λ = 0.7092 Å, a MAR345 2D-image plate detector for the first series of experiments; λ = 0.68239 Å, Pilatus 2M hybrid pixel detector for the second series of experiments). The beam was slit-collimated down to 100−150 μm. Nominal sample-to-detector distances (200 and 193 mm, respectively), coordinates of beam center, and detector tilts were calibrated using LaB_6 (NIST standard 660b) loaded in the DAC of the same type without applying pressure. The exposure time was varied between 180 and 1000 s.

A structural study in the pressure range up to 30 GPa was performed by X-ray diffraction using synchrotron radiation (λ = 0.5635 Å) at Beamline 01C2 of National Synchrotron Radiation Research Center (NSRRC), Hsinchu, Taiwan. The fine powder sample was loaded into DAC (flat culets of 0.5 mm size) in a hole (0.2 mm diameter) drilled in a preindented (0.040 mm thickness) stainless steel gasket under a high-purity argon atmosphere. Several ruby spheres were loaded along with the sample and were used for pressure estimation. No pressure-transmitting medium was used.

Raw powder diffraction data were processed (calibration, masking of the reflections from diamond and ruby, integration) using the Fit2D program.[29] Uncertainties of the integrated intensities were calculated at each 2θ point by applying Poisson statistics to the intensity data considering the geometry of the 2D detector.[30,31]

Temperature-Variable SR-XPD. A powdered sample of δ-$Mn(BH_4)_2$ produced in the steel press (S3) was mounted in a sapphire (Al_2O_3) single-crystal tube (o.d., 1.09 mm; i.d., 0.79 mm) in an argon-filled glovebox $p(O_2, H_2O)$ < 1 ppm and placed in a specially developed in situ sample cell for investigation of solid−gas reactions.[32] The temperature was controlled with a thermocouple placed in the sapphire tube in direct contact with the sample. The samples were heated at a rate of 5 °C/min between RT and 400 °C in p(Ar) ≈ 1 bar and $p(H_2)$ ≈ 100 bar. In situ SR-XPD data were collected at beamline I711 at the MAX IV laboratories in Lund, Sweden with a MAR165 CCD detector system with X-ray exposure times of 30 s and a selected wavelength of λ = 0.9919 Å. The raw 2D diffraction data sets were

DOI: 10.1021/acs.chemmater.5b04102
Chem. Mater. 2016, 28, 274−283

transformed to powder patterns using the Fit2D program, incorporating wavelength calibration using a NIST 660a LaB_6 standard, and masking single-crystal diffraction spots from the sapphire sample holder.[29] Uncertainties of the integrated intensities were calculated at each 2θ point by applying Poisson statistics to the intensity data considering the geometry of the detector.[31]

Structure Determination. The structure of δ-$Mn(BH_4)_2$ was initially refined in the $P4_2nm$ space group simply by using the previously reported crystal structure of δ-$Mg(BH_4)_2$ as an initial model (replacing Mg atom for Mn). However, DFT calculation reveals that the structure in the $P4_2nm$ space group shows five imaginary normal modes. The simulated annealing was performed for structures in $P4_2nm$ symmetry and pressures of 2, 4, 6, and 8 GPa. This led to a new structure with the same complexity ($Z = 2$) but with a significantly smaller c/a ratio. The new structure is stable with respect to atomic displacements in the pressure range from 3 to 9 GPa. Above this pressure, a single imaginary mode was present. Imposing the atomic displacements related to the imaginary mode results in $Pnn2$ structure with $Z = 2$. A continuous phase transition was observed theoretically between $P4_2nm$ and $Pnn2$ structures around 9.2 GPa. The $Pnn2$ structure annealed by DFT at ambient pressure results in a new structure with $P\text{-}4n2$ symmetry. This structure is stable in the pressure range from 0 to 1.5 GPa (see Supporting Information). However, a structure in the same $\sqrt{2}a \times 2c$ supercell but with $I4_1/acd$ ($Z = 8$) symmetry does not have any phonon instabilities between 1 and 10 GPa. At ambient pressure, a soft phonon is present at the point X of the Brillouin zone (see the Supporting Information). At higher pressures, we have not found soft modes for this structure below 18 GPa. Above this pressure, 4 soft phonons are present. The $P\text{-}4n2$ and $I4_1/acd$ structures optimized theoretically show c/a ratios similar to the experimental values found for the subcell.

A comparison of the ground state energies reveals that below 1.5 GPa the $P3_112$ α-$Mn(BH_4)_2$ structure is preferred; just above 1.5 GPa, both $P\text{-}4n2$ and $I4_1/acd$ have the lowest ground state energy with a preference for the latter at higher pressures. For pressures higher than 10 GPa, the $Fddd$ structure is the most stable. Although two structures, $Pnn2$ and $P4_2nm$, are stable with respect to atomic displacements, they are energetically unfavorable in any pressure range. One has to keep in mind that the present calculations inherently contain simplification related to the magnetic ordering. The more complex antiferromagnetic order would change the energy of the system; thus, the ground state energy comparison is only qualitative.

Theoretically determined structures were refined by the Rietveld method using Fullprof Suite software.[33] The positions of the manganese atoms are nonparametric, and the coordinates of the B and H atoms were refined using soft constraints on the B−H distances (1.12 Å). Atomic displacement parameters were refined for each type of atom. A preferred orientation was modeled by applying March−Dollase approximation for the (001) direction, and an orthorhombic strain was modeled for the tetragonal lattice. The models for the δ-phase were refined sequentially in a whole pressure range of existence. Such a combined structural search suggests that the first high-pressure phase, δ-$Mn(BH_4)_2$, is isostructural to the high-pressure phase of δ-$Mg(BH_4)_2$.[18] The stable structures in the $P\text{-}4n2$ and $I4_1/acd$ space groups ($\sqrt{2}a \times 2c$ supercell compared to the initial $P4_2nm$ structure) have similar refinement indicators; thus, none can be ruled out. The only indication for the preference comes from the dispersion relations (Supporting Information). At ambient pressure, $P\text{-}4n2$ is stable with respect to atomic displacements, and above 1.5 GPa, the $I4_1/acd$ structure has no imaginary normal modes.

Appearance of a new diffraction peak at low angles clearly indicates another phase transformation at around 9 GPa. We started from the assumption that the new phase, δ'-$Mn(BH_4)_2$, is a deformation of the δ-phase, so we tested different indexing solutions that would represent the supercells. The subgroups of $P4_2nm$ with doubled c parameter were tested, and with the systematic absences of reflections taken into account, the $I4_1md$ group was initially chosen. The $P4_2nm$ model of δ-$Mn(BH_4)_2$ transformed the space group $I4_1md$ with the $\sqrt{2}a \times 2c$ cell using PowderCell.[34] We used this model in the initial Rietveld refinement of δ'-$Mn(BH_4)_2$. However, this candidate structure with $I4_1md$ symmetry is not stable in the pressure range 0−18 GPa with numerous imaginary normal modes, which inspired our further search for more suitable structures. To find the symmetry of δ'-$Mn(BH_4)_2$, we have performed additional simulated annealing searches constructing superstructures with $Z = 8$ in a primitive cell for all of the structures considered above. This procedure reveals that the $\sqrt{2}a \times 2c$ supercell leads to two stable symmetries: $P2_1/c$ in the $\sqrt{2}a \times 2c$ supercell ($Z = 8$) and $Fddd$ in the $2a \times 2c$ supercell ($Z = 16$). The final structure, which is stable and describes the X-ray powder pattern well, was found in the orthorhombic $Fddd$ space group with all three unit cell parameters doubled compared to the starting $P4_2nm$ model ($2a \times 2b \times 2c$).

The model of δ'-$Mn(BH_4)_2$ was refined in the $Fddd$ space group. The Mn atom was placed in the x, 1/8, 1/8 position with one refined coordinate. The coordinates of BH_4^-, the thermal factors for each type of atom, and the preferred orientation in the (001) direction were refined. The structure of the δ'-polymorph was refined sequentially for all higher pressure points.

DFT Calculations. The calculations were performed within the density functional theory (DFT) formalism with periodic plane wave expansion of the electronic wave functions implemented in the Vasp package.[35,36] Electronic configuration of $3d^64s^1$ for Mn, $2s^22p^1$ for B, and $1s^1$ for H was represented by projected augmented wave potentials.[37] The gradient corrected (GGA) functional[38] was used for the exchange correlation functional. The DFT within the standard GGA approximation to the exchange and correlation functional is known to suffer limitations in describing the physics of magnetic materials with strongly localized electronic states. This is mostly due to the spurious, self-interaction of the localized electrons, such as the Mn d states in $Mn(BH_4)_2$, where Mn occurs in a +2 oxidation state. In the present studies, we have applied a DFT+U (GGA+U) approach to circumvent the self-interaction problem. The concept of the DFT+U approach is related to addressing the on-site Coulomb interactions in the localized d or f orbitals with an additional Hubbard-type term in the Hamiltonian. We have applied the DFT+U method developed by Anisimov et al.[39] In this approach, an effective interaction parameter $U_{eff} = U - J$ (further denoted as U) is introduced. Following reports for MnO, where Mn has the same oxidation state as in $Mn(BH_4)_2$, we have applied $U = 4$.[40,41] It is well-known that a more advanced theoretical description appears to be superior with respect to GGA+U for Mott−Hubbard type insulators;[40] however, the computational costs related to these methods would make a search for the ground state structures intractable. The test calculations without Hubbard correction for the α-$Mn(BH_4)_2$ give unrealistic magnetic moments on Mn, structure, and the very small band gap (<1 eV); therefore, all of our calculations were performed with the GGA+U method as described above. To avoid complications with ordering of the magnetic states on Mn for all calculations, the ferromagnetic order was assumed. In fact, this simplification does not properly describe the symmetry that might be related to other magnetic ordering in $Mn(BH_4)_2$; however, the X-ray diffraction technique used within the present study is insensitive to the ordering of the magnetic moments. The antiferromagnetic order for the $P\text{-}4n2$ phase indeed has the ground state energy lower by 0.02 eV per formula unit than the ferromagnetic one, and the volume of the unit cell differs by 0.6%. This defines the accuracy of the present calculations.

Static structural optimization was performed with the conjugate gradient method; for each given pressure, internal atomic positions as well as the lattice parameters were optimized until forces excerpted on atoms were smaller than 0.001 eV/Å. The crystal symmetry was constrained during this process. Once the structure has converged, the normal-mode analysis was performed. For simplicity, the normal-mode frequencies were calculated at the Γ point by displacing the symmetry-inequivalent atoms in all crystallographic directions by ±0.01 Å. To check this approach for selected configurations, we have used the linear response method. The results of both approaches differ up to a few percent. For the ultimate stability test, the phonon dispersion relations were determined in the whole Brillouin zone for all candidate structures. The real space method was applied,[42] and the forces excerpted on atoms were calculated with the linear response method in

DOI: 10.1021/acs.chemmater.5b04102
Chem. Mater. 2016, 28, 274−283

the suitable supercells with 16 or 32 formula units. For the phonon calculations, various ordering of Mn magnetic moments were taken into account in separate calculations. In particular at lower pressures, the antiferromagnetic ordering provides relations without soft phonons; thus, the antiferromagnetic state is taken into account in phonon dispersion relations for *P*-4*n*2 and $I4_1/acd$. All calculations related to the vibrational properties were performed within the GGA +U method.

For structures with imaginary modes, simulated annealing was performed to find new stable atomic configurations. This was done by heating the structure to T = 200−300 K at a rate of 100 K/ps and cooling it to T = 0 K at a rate of 50 K/ps. No constraints were imposed on the internal atomic positions; the unit cell parameters were kept fixed during the annealing process. The Nose−Hoover thermostat[43,44] was applied for this procedure, and the time step for integration of equations of motion was 0.6 fs. The symmetry of the system was analyzed[45] after each annealing step. Any new symmetry was optimized with methods used for the static calculations, and normal modes were analyzed. Superstructures with various multiplications of the unit cell were considered for the simulated annealing process if appropriate.

The magnetic moment of Mn is 4.60 μ_B for $P3_112$ structure at 0 GPa, 4.59 μ_B for *P*-4*n*2 at 2 GPa, 4.58 μ_B for $I4_1/acd$ structure at 4 GPa, and 4.56 μ_B for *Fddd* structure at 10 GPa. All structures are insulating with the band gap ranging between 3.7 eV in the $P3_112$ structure at 0 GPa and 2.9 eV for the $I4_1/acd$ structure at 8 GPa; see the electronic density of states in the Supporting Information. In fact, the band gap also depends on the magnetic ordering of Mn ions; however, magnetic properties are beyond the scope of the present report.

RESULTS AND DISCUSSION

1. Structure of δ-Mn(BH$_4$)$_2$. The two identified structural models for δ-$Mn(BH_4)_2$ are different variants of BH_4 orientational order that are more stable than the initial guess $P4_2nm$ structure.[18] The *P*-4*n*2 structure has the same cell, whereas the $I4_1/acd$ structure is built in the $\sqrt{2}a \times 2c$ supercell. Even good quality powder diffraction data obtained for δ-$Mn(BH_4)_2$ in the ex situ synchrotron experiment at ambient conditions do not reveal superstructure peaks nor do they show better fit for one of the models. The two models differ only by the orientation of the BH_4 groups, whereas Mn atoms (these atoms make the largest contribution to the structure factors) occupy equivalent nonparametric special positions. Thus, X-ray powder diffraction and DFT calculations are more consistent with the *P*-4*n*2 structure. However, more arguments on the choice of the space group will be given in section 3 following the theory of phase transitions.

The structure of δ-$Mn(BH_4)_2$ consists of two interpenetrated $Mn(BH_4)_2$ frameworks, being the tetragonally deformed Cu_2O antitype, similar to its analogues δ-$Mg(BH_4)_2$[18] and α-$Cd(BH_4)_2$.[46] δ-$Mn(BH_4)_2$ has no voids in the structure and shows high volumetric density of hydrogen of 125 g H_2/L at ambient conditions. A complex orientational order of BH_4^- anions may take place in metal borohydrides at high pressures, reducing repulsive H···H interactions between the anions. For example, it was shown that the *Ama*2 structure of $LiBH_4$ determined from X-ray powder diffraction at high pressures[11] has a higher energy than its $I4_1/acd$ substructure in the $\sqrt{2}a \times 2c$ supercell, predicted theoretically.[47] Later, the same $I4_1/acd$ ordering pattern of the BH_4 groups in the $\sqrt{2}a \times 2c$ supercell had been proposed for the high-pressure phase of magnesium borohydride.[48] The order of hydrogen atoms is not manifested in the X-ray powder data; it is especially difficult to see it from high pressure data, but it can be suggested from energy calculations, determined directly, or simply confirmed by neutron powder diffraction. The high-pressure neutron diffraction study of $Mn(BH_4)_2$ is out of scope of this work, especially in view of a possible contribution of magnetic ordering for Mn^{2+} ions, but we rely on DFT for optimization of hydrogen atoms positons. Both optimized models give reasonable structures: no short H−H contacts, usual coordination of BH_4^- groups to Mn via edges, and similar ground state energies. At ambient pressure, the *P*-4*n*2 structure has no soft modes, whereas at pressures above 1.5 GPa, the $I4_1/acd$ structure is stable with respect to atomic displacements. The energy difference between them is negligible, especially because more complicated magnetic order may be present at very low temperatures (which is beyond the scope of this study). At 0 GPa, the $P3_112$ structure has the lowest energy, and both candidate structures for δ-$Mn(BH_4)_2$ are metastable. The cell parameters of the δ-$Mn(BH_4)_2$ structure at ambient conditions refined in the space group $I4_1/acd$ are a = 7.85245(6), c = 12.1456(2) Å, and V = 748.91(1) Å^3.

2. Structure of δ′-Mn(BH$_4$)$_2$. The structure of δ′-$Mn(BH_4)_2$ is very similar to the δ-polymorph and is also comprised of two interpenetrated $Mn(BH_4)_2$ frameworks. The two frameworks in the δ′-phase are crystallographically independent and thus are slightly shifted relative to each other (see Figure 3), giving rise to the superstructure peaks in the diffraction patterns. The cell parameters of the δ′-$Mn(BH_4)_2$ structure at 11.8 GPa refined in the space group *Fddd* are a = 9.205(17), b = 9.321(10), c = 12.638(15) Å, and V = 1084(3) Å^3.

The structure of δ′-$Mn(BH_4)_2$ does not explain the observed powder pattern of the second high-pressure phase of $Mg(BH_4)_2$ (denoted ε-phase in the Supporting Information to ref 18), thus showing that δ′-$Mn(BH_4)_2$ is not isostructural to ε-$Mg(BH_4)_2$.

3. High-Pressure Behavior of Mn(BH$_4$)$_2$. Synchrotron radiation X-ray powder diffraction shows that the first phase transition in $Mn(BH_4)_2$ occurs in the range of 0.5−2.0 GPa, where the initial α-phase and the emerging high-pressure δ-phase coexist. This coexistence is typical for the first order phase transition and the coexistence range differs slightly in various experiments.

The structure of α-$Mn(BH_4)_2$ is characterized by a significant amount of empty space.[22] During the first phase transition, α-$Mn(BH_4)_2$ collapses, losing 16% of the volume, and rearranges to δ-$Mn(BH_4)_2$ (see Figure 2). Calculations do not exclude the possibility that in the narrow pressure range of 0−1.5 GPa a metastable *P*-4*n*2 structure exists.

The second phase transition from δ-phase to δ′-phase occurs near 8.5−11.5 GPa in both experiments and results in a few additional peaks in the diffraction pattern that indicate a superstructure, apparently emerging from ordered displacements of the two frameworks. The δ′-$Mn(BH_4)_2$ phase remains stable up to at least 17.2 GPa according to the Raman spectroscopy data but did not persist after decompression. High-pressure diffraction experiments performed at NSRRC show that δ′-$Mn(BH_4)_2$ is stable up to 29.4 GPa, yielding the cell parameters a = 8.545(7) Å, b = 8.832(5) Å, and c = 12.966(9) Å (see the Supporting Information).

Both δ- and δ′-phases on compression expand along the c axis and shrink in the other two directions (see Figure 2). The unit cell volumes for α- and δ-phases were fitted by the Murnaghan equation of state

DOI: 10.1021/acs.chemmater.5b04102
Chem. Mater. 2016, 28, 274−283

$$V(P) = V_0\left(1 + B_0'\frac{P}{B_0}\right)^{-1/B_0'}$$

where B_0 is a bulk modulus, B'_0 is the first pressure derivative of bulk modulus (fixed at 5.8 for all phases), and V_0 is the molar volume at zero pressure. Variation of the volume of the $Mn(BH_4)_2$ formula unit for the α- and δ-phases is shown in Figure 1. The bulk moduli for the α- and δ-phases of

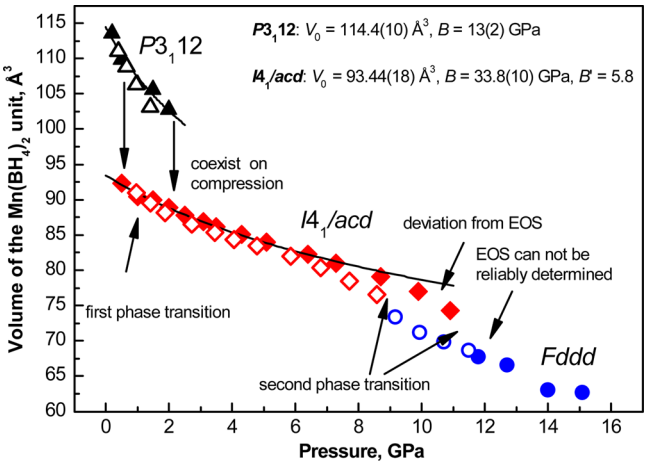

Figure 1. Volume of $Mn(BH_4)_2$ formula unit relative to pressure. Filled symbols show results of the experiment on the LiCl-containing sample; empty symbols, on the $NaBH_4$-containing sample; black symbols, α-phase; red symbols, δ-phase; and blue symbols, δ'-phase. Equations of state were calculated using data from the experiment on the LiCl-containing sample.

$Mn(BH_4)_2$ (13 and 33.8 GPa, respectively) are slightly higher than for the α- and δ-phases of $Mg(BH_4)_2$ (10.2 and 28.5 GPa, respectively).

The available powder diffraction data do not reveal a significant change of volume during the second phase transition (Figure 1) but show almost a continuous change of the cell parameters with pressure, as shown in Figure 2. For this phase transition to be of second order (at different temperatures, for

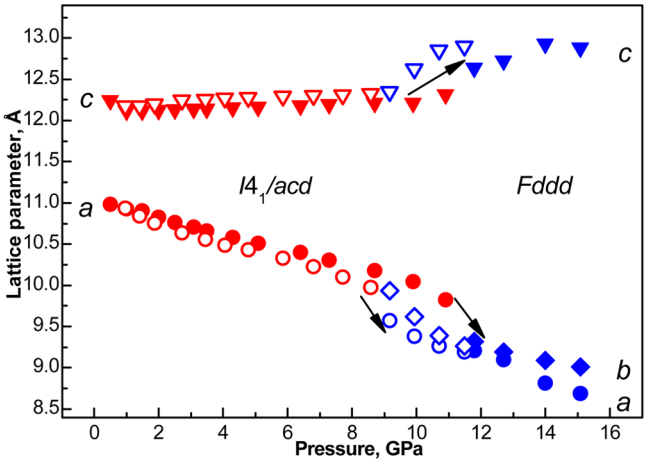

Figure 2. Lattice parameters of high-pressure phases of $Mn(BH_4)_2$. To put the values on the same scale, the cell parameter a of the δ-phase was multiplied by $\sqrt{2}$. Filled symbols show the results for the LiCl-containing sample; empty symbols, for $NaBH_4$-containing sample; red symbols, δ-phase; and blue symbols, δ'-phase.

example), the symmetry of the δ and δ' structures should be linked as group−subgroup of the lowest index. This is possible if we assume $I4_1/acd$ symmetry for the δ-phase. Indeed, the $Fddd$ symmetry in the unit cell $2a \times 2a \times 2c$ (referring to the a and c of the parent $P4_2nm$ phase) is the direct subgroup of $I4_1/acd$ with the unit cell $\sqrt{2}a \times \sqrt{2}a \times 2c$. Thus, our final choice of the space group, based on powder diffraction experiments, DFT calculations, and symmetry analysis suggests $I4_1/acd$ symmetry for the δ-phase. The other option, $P\text{-}4n2$, might be valid too, subject to a neutron diffraction study.

Finally, we suggest the following sequence of phase transitions for $Mn(BH_4)_2$: α-$Mn(BH_4)_2$ ($P3_112$) transforms to δ-$Mn(BH_4)_2$ ($I4_1/acd$) in the range 0.5−2.0 GPa, which transforms to δ'-$Mn(BH_4)_2$ ($Fddd$) at approximately 8.5−11.5 GPa. However, in the pressure range from 0 to 1.5 GPa, a metastable $P\text{-}4n2$ structure may also occur because according to the calculations it is stable with respect to atomic displacements, whereas the $I4_1/acd$ structure has no imaginary normal modes only above 1.5 GPa.

4. Influence of LiCl and the Possibility of Anion Exchange between LiCl and $Mn(BH_4)_2$ at High Pressures. Hypothetically, an anion exchange can take place, giving rise to mixed-anion borohydride $Mn(BH_4)_{2-x}Cl_x$. The existence of mixed-anion borohydrides has recently been documented,[49−60] but to our knowledge no direct anion exchange under high

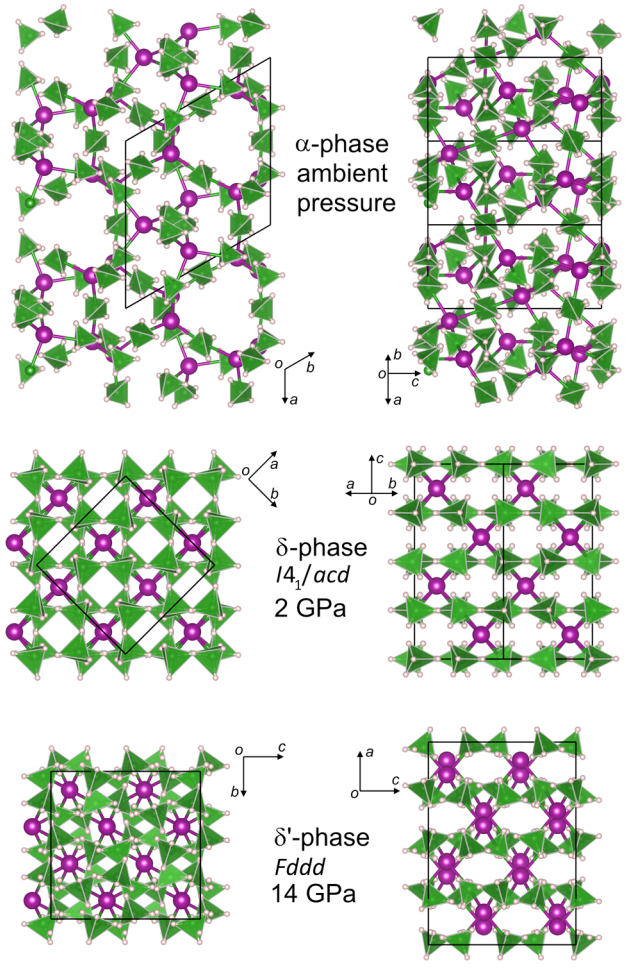

Figure 3. Fragments of crystal structures of the ambient pressure α-$Mn(BH_4)_2$ and high-pressure δ- and δ'-$Mn(BH_4)_2$. Manganese cations are shown as purple spheres, BH_4^- groups as green tetrahedra.

DOI: 10.1021/acs.chemmater.5b04102
Chem. Mater. 2016, 28, 274−283

pressure has been reported to date for any metal borohydride. The presence of Cl^- in the structure should change intensities of powder diffraction peaks compared to the native $Mn(BH_4)_2$, but if x is small the difference in the intensities might be hard to detect, especially in the case of a high-pressure powder diffraction experiment. However, comparing the results of the high-pressure experiment on samples containing LiCl and $NaBH_4$ allows us to compare the evolution of the formula volumes. Because the Cl^- anion takes a smaller volume than BH_4^-, the resulting unit cell volume of $Mn(BH_4)_{2-x}Cl_x$ should be smaller than that of $Mn(BH_4)_2$. However, Figure 1 does not reveal a difference of the unit cell volumes between the Cl-free and Cl-containing samples, thus showing no evidence for anion exchange.

We found a significant difference in the pressure ranges for the second phase transition. For the LiCl-containing sample, the second phase transition occurs between 10.9 and 11.8 GPa according to the X-ray powder diffraction data and between 10.1 and 11.8 GPa according to the Raman data, whereas the $NaBH_4$-containing sample undergoes the second phase transition at a lower pressure between 8.59 and 9.17 GPa (see Figures 1 and 2). These differences in the pressure can be explained by the fact that a large amount of LiCl (50 wt %) or $NaBH_4$ (31 wt %) may serve as pressure-transmitting media with different properties.

5. High-Pressure Raman Spectroscopy. The presence of LiCl has no impact on Raman data, as it generates no first order Raman spectrum due to its cubic structure (space group $Fm\text{-}3m$), and the second order spectrum is in the range 50−650 cm^{-1}[161] beyond the accessible $Mn(BH_4)_2$ spectrum. Conversely, as discussed above, the Cl^- anion from LiCl could be involved in anion exchange with the BH_4^- group from $Mn(BH_4)_2$ and thus might slightly influence the observed frequencies.[62] Results of the Raman measurements agree well with the X-ray powder diffraction data: the first spectrum measured at 1.4 GPa differs from the ambient pressure spectrum of $Mn(BH_4)_2$, indicating that the first phase transition has already completed. The spectrum at 1.4 GPa shows (Figure 4) a splitting of the peak at 2271 cm^{-1} (stretching mode of BH_4^-), which was not observed at the ambient pressure. The Raman spectrum of the δ-phase changes continuously from 1.4 to 10.1 GPa and then undergoes a discrete change between 10.1 and 11.8 GPa, indicating the second phase transition. The peak that was observed at 2161 cm^{-1} at ambient pressure (marked with an asterisk in Figure 4) continuously shifts to higher wavenumbers upon compression and almost disappears before the second phase transition. The shape of the strongest peak at 2271 cm^{-1} changes significantly within the existent range of the δ-phase, most likely due to an anisotropic compression of the structure resulting in different values of $d\nu/dP$ for these bands. It looks like the bending mode at ~1150 cm^{-1} disappears and appears again during compression, but it could just be associated with a variation of the intensity of this weak peak. Once the second phase transition occurs, the Raman spectrum of the resulting δ'-$Mn(BH_4)_2$ changes continuously until 17.1 GPa, which was the highest pressure reached; these data indicate that the δ'-phase is stable up to at least 17.1 GPa.

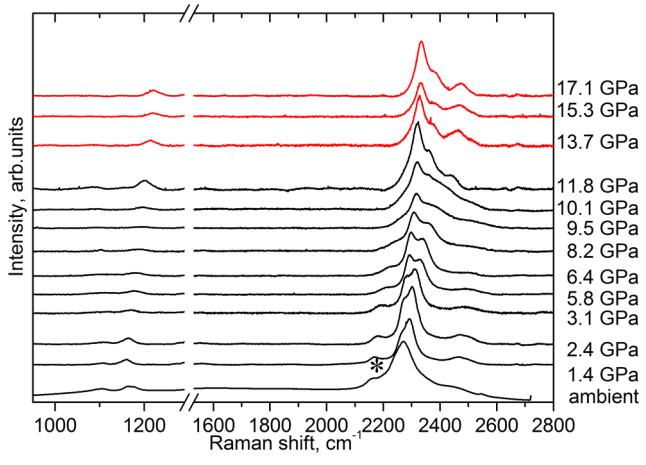

Figure 4. Raman spectra of $Mn(BH_4)_2$ high-pressure phases (black lines, δ-polymorph; red lines, δ'-polymorph). The background was subtracted for clarity. The data at ambient pressure are taken from ref 22.

6. Synthesis of δ-$Mn(BH_4)_2$ in a Large-Volume Steel Press. The low pressure of formation and the metastability of δ-$Mn(BH_4)_2$ at ambient conditions allow for its preparation in bulk. δ-$Mn(BH_4)_2$ was recently observed to form in ball milling $Mn(BH_4)_2$-MBH_4 (M = Li and Na) mixtures.[63] In this work, we used a large-volume steel press to produce a larger sample of the δ-phase and to study its thermal behavior. Analysis of the SR-XPD data obtained at room temperature (the bottom pattern in Figure 5) revealed 96 wt % of δ-$Mn(BH_4)_2$ and 4 wt

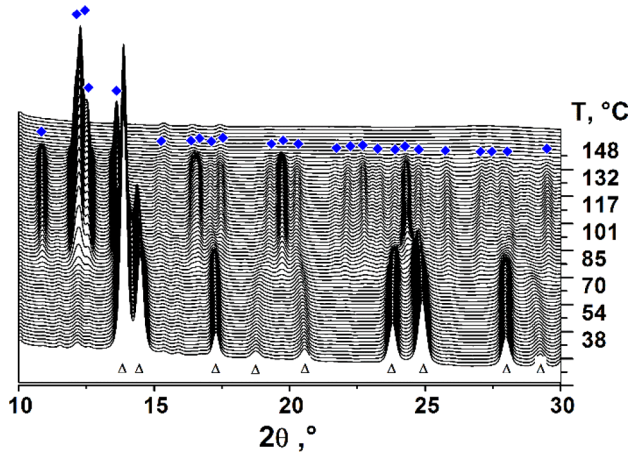

Figure 5. In situ SR-XPD on δ-$Mn(BH_4)_2$ (S3) heated from RT to 160 °C, λ = 0.9919 Å. Symbols: Δ, δ-$Mn(BH_4)_2$; ♦, α-$Mn(BH_4)_2$.

% of α-$Mn(BH_4)_2$, i.e., almost complete transition. The high pressure polymorph remains stable at room temperature over at least several months.

To verify the effect of LiCl, we investigated sample S4 consisting of α-$Mn(BH_4)_2$ with 50 wt % of LiCl by XPD after two 3 h long compressions at 1.2 GPa. It also shows an almost complete phase transition from α-$Mn(BH_4)_2$ to δ-$Mn(BH_4)_2$ while LiCl remains unchanged (Figure 6). The δ-$Mn(BH_4)_2$ polymorph in the presence of the chloride is also stable at ambient conditions. Thus, LiCl does not influence the formation and stability of δ-$Mn(BH_4)_2$.

7. Thermal Behavior of δ-$Mn(BH_4)_2$. In situ synchrotron X-ray powder diffraction was used to investigate the thermal behavior of δ-$Mn(BH_4)_2$ (S3) upon heating (Figure 5). A significant anisotropic thermal expansion is observed for δ-$Mn(BH_4)_2$: the sequential Rietveld refinement showed that the unit cell expands along the a axis while the c axis contracts (see Figure 7), which is similar to the behavior seen for the lighter δ-

DOI: 10.1021/acs.chemmater.5b04102
Chem. Mater. 2016, 28, 274−283

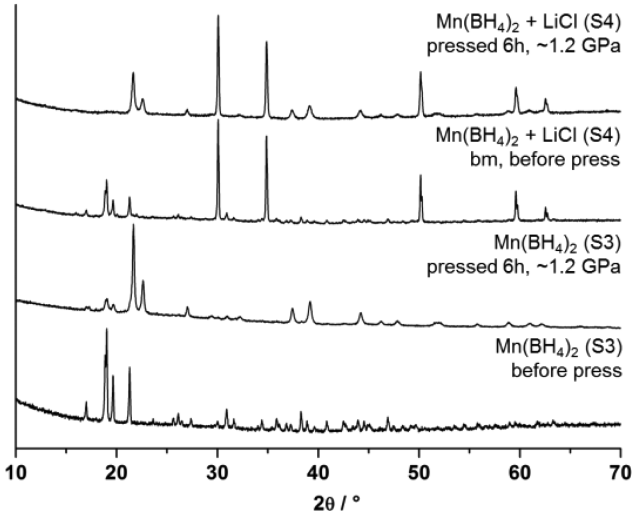

Figure 6. XPD data of $Mn(BH_4)_2$ (S3) and $Mn(BH_4)_2$ with 50 wt % of LiCl (S4) before and after two 3 h periods at ~1.2 GPa with Cu $K\alpha_1$.

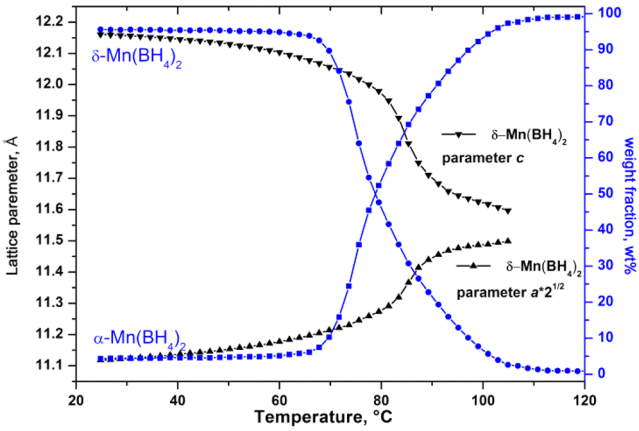

Figure 7. Temperature evolution of the unit cell parameters of δ-$Mn(BH_4)_2$ and of the weight fractions of the two polymorphs from the sequential Rietveld refinement on the in situ SR-XPD data. To put the values on the same scale, we multiplied the cell parameter a of the δ-phase by $\sqrt{2}$.

$Mg(BH_4)_2$.[18] Upon heating, δ-$Mn(BH_4)_2$ tends to reach the ideal cubic symmetry of the Cu_2O prototype actually observed for β-$Cd(BH_4)_2$,[46] but it does not reach it below the decomposition temperature of $Mn(BH_4)_2$. Smaller ionic radius of Mn compared to Cd presumably leads to stronger repulsion between the borohydride anions, and thus, the structure is stabilized in the lower tetragonal symmetry.

The intensities of diffraction peaks from δ-$Mn(BH_4)_2$ begin to decrease at T = 67 °C and completely disappear at T = 109 °C, whereas the intensities of α-$Mn(BH_4)_2$ simultaneously increase. The weight fractions of both polymorphs extracted from the sequential Rietveld refinement are plotted as a function of temperature in Figure 7. At T = 124 °C, the diffraction peaks from α-$Mn(BH_4)_2$ start to decrease and disappear at T = 146 °C. The same sample was also decomposed under 100 bar of H_2. The diffraction peaks' intensities of δ-$Mn(BH_4)_2$ begin to decrease at T = 68 °C and disappear at T = 100 °C, whereas the intensity of α-$Mn(BH_4)_2$ increases in the same temperature range. At T = 118 °C, the peaks from α-$Mn(BH_4)_2$ start to decrease and disappear at T = 135 °C.

The thermal analysis of δ-$Mn(BH_4)_2$ (S3) by combined TGA-DSC-MS reveals (Figure 8) a broad endothermic DSC

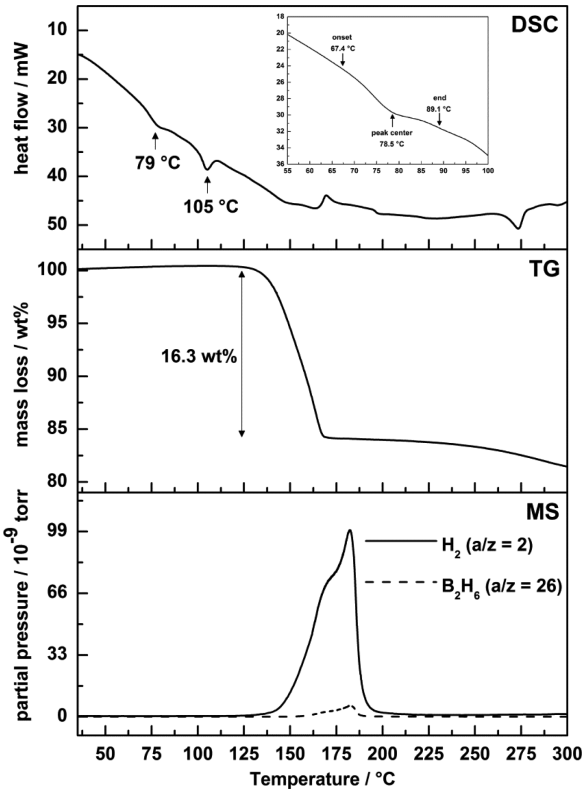

Figure 8. Thermal analysis of δ-$Mn(BH_4)_2$ (S3) heated from RT to 300 °C at 5 °C/min, combining differential scanning calorimetry with a zoom-in on the first endothermic peak (top), thermogravimetry (middle), and mass spectrometry (bottom).

diffraction peaks between 67 and 89 °C, with the weighted center at 79 °C, which is attributed to the polymorphic transition from δ- to α-$Mn(BH_4)_2$. No mass loss or gas release is detected by TGA or MS in this temperature region. Another endothermic event is observed at 105 °C, which is related to the polymorphic transformation from the orthorhombic to the hexagonal $LiBH_4$ present as an impurity in the sample.[64,65] At 130 °C, the sample begins to decompose and releases a mixture of hydrogen and diborane gas, resulting in a mass loss of 16.3 wt % between 130 and 200 °C. This decomposition behavior is in agreement with a previous report for α-$Mn(BH_4)_2$.[7] A photographic study reveals the decomposition of α-$Mn(BH_4)_2$ without melting for slow heating rates similar to those used here, but very rapid heating, e.g., at ~10 °C/s (using a heat gun) clearly allows for a molten phase prior to the decomposition.[8] Sample S4 was also investigated and shows the same thermal behavior although with a reduced mass loss (8.9 wt % between 130 and 200 °C) and gas release and less pronounced DSC peaks due to the presence of inert LiCl in the sample (data not shown).

Thus, we conclude that the δ-phase is not providing a gain in hydrogen storage temperatures, as the decomposition occurs via an intermediate formation of the ambient pressure α-phase. The polymorphic transition from δ- to α-$Mn(BH_4)_2$ and the decomposition of α-$Mn(BH_4)_2$ under 1 bar of argon and under

DOI: 10.1021/acs.chemmater.5b04102
Chem. Mater. 2016, 28, 274−283

100 bar of H_2 back-pressure proceed similarly. However, δ-$Mn(BH_4)_2$ provides one of the highest volumetric densities of hydrogen of 125 g H_2/L at ambient conditions.

CONCLUSIONS

X-ray powder diffraction and Raman spectroscopy experiments on α-$Mn(BH_4)_2$ in DACs reveal two phase transitions under pressure. The crystal structure of the new polymorphs was determined with the aid of ab initio calculations. The first transition to δ-$Mn(BH_4)_2$ ($I4_1/acd$ or $P\text{-}4n2$ space group symmetry) occurs near 1 GPa similar to its Mg analogue, closing the empty voids in the α-phase structure. The second transition from δ-$Mn(BH_4)_2$ to δ'-$Mn(BH_4)_2$ ($Fddd$ space group, different from the one in the Mg-based system) occurs in the pressure range of 8.6−11.8 GPa. During the second phase transition, the two interpenetrated frameworks are shifted relative to each other, resulting in additional superstructural peaks in the diffraction pattern of the δ'-phase. The δ-phase remains stable under decompression to ambient conditions, at least for a few months. It can also be obtained by ball milling or a compression of α-$Mn(BH_4)_2$ in a large-volume press. Heating in argon (1 bar) or hydrogen (100 bar) atmosphere leads to a gradual transformation of δ-$Mn(BH_4)_2$ back to α-$Mn(BH_4)_2$ in the temperature range 67−109 °C, the latter in turn starts to decompose at 130 °C with the release of mostly hydrogen. Despite δ-$Mn(BH_4)_2$ not providing an advantage in hydrogen desorption temperature, it yields a high volumetric density of hydrogen of 125 g H_2/L under ambient conditions.

ASSOCIATED CONTENT

Supporting Information

The Supporting Information is available free of charge on the ACS Publications website at DOI: 10.1021/acs.chemmater.5b04102.

Rietveld refinement plots, total energy calculations relative to pressure, the equations of state, and phonon dispersion curves (PDF)

Crystallographic information (CIF)

AUTHOR INFORMATION

Corresponding Author

*E-mail: yaroslav.filinchuk@uclouvain.be.

Notes

The authors declare no competing financial interest.

ACKNOWLEDGMENTS

The authors thank FNRS (CC 1.5169.12, PDR T.0169.13, EQP U.N038.13) for financial support. We acknowledge the Fonds Spéciaux de Recherche (UCL) for the incoming postdoctoral fellowship cofunded by the Marie Curie actions of the European Commission granted to N.A.T. We thank ESRF, Grenoble, France for the beamtime allocation at the SNBL, as well as the beamline I711 at the MAX-II synchrotron, Lund, Sweden, and the beamline I11 at the Diamond Light Source, Didcot, UK. Part of this work was supported by the Danish National Research Foundation, Center for Materials Crystallography (DNRF93), the Innovation Fund Denmark (project HyFill-Fast), and by the Danish Research Council for Nature and Universe (Danscatt). We are grateful to the Carlsberg Foundation. Part of this work was supported by the COST Action MP1103 "Nanostructured materials for solid-state hydrogen storage". Z.Ł. acknowledges CPU allocation at the PLGrid Infrastructure and support by a grant from Switzerland through the Swiss Contribution to the enlarged European Union. R.Č. acknowledges support from the Swiss National Science Foundation. T.P. gratefully acknowledges the support of the Polish National Science Centre within Project 2011/01/M/ST3/00855 (program "Harmonia") and the valuable help of Dr. J.J. Lee and E. Magos-Palasyuk during measurements at 01C2 beamline (NSRRC, Hsinchu, Taiwan).

REFERENCES

(1) Li, H.-W.; Yan, Y.; Orimo, S.; Züttel, A.; Jensen, C. M. Recent Progress in Metal Borohydrides for Hydrogen Storage. *Energies* **2011**, *4*, 185−214.

(2) Ravnsbæk, D. B.; Filinchuk, Y.; Cerný, R.; Jensen, T. R. Powder Diffraction Methods for Studies of Borohydride-Based Energy Storage Materials. *Zeitschrift für Krist.* **2010**, *225*, 557−569.

(3) Rude, L. H.; Nielsen, T. K.; Ravnsbaek, D. B.; Bösenberg, U.; Ley, M. B.; Richter, B.; Arnbjerg, L. M.; Dornheim, M.; Filinchuk, Y.; Besenbacher, F.; Jensen, T. R. Tailoring Properties of Borohydrides for Hydrogen Storage: A Review. *Phys. Status Solidi A* **2011**, *208*, 1754−1773.

(4) Ley, M. B.; Jepsen, L. H.; Lee, Y.-S.; Cho, Y. W.; Bellosta von Colbe, J. M.; Dornheim, M.; Rokni, M.; Jensen, J. O.; Sloth, M.; Filinchuk, Y.; Jørgensen, J. E.; Besenbacher, F.; Jensen, T. R. Complex Hydrides for Hydrogen Storage − New Perspectives. *Mater. Today* **2014**, *17*, 122−128.

(5) Schrauzer, G. N. Über Ein Periodensystem Der Metallboranate. *Naturwissenschaften* **1955**, *42*, 438.

(6) Nakamori, Y.; Miwa, K.; Ninomiya, A.; Li, H.; Ohba, N.; Towata, S.; Züttel, A.; Orimo, S. Correlation between Thermodynamical Stabilities of Metal Borohydrides and Cation Electronegativites: First-Principles Calculations and Experiments. *Phys. Rev. B: Condens. Matter Mater. Phys.* **2006**, *74*, 045126.

(7) Liu, R.; Reed, D.; Book, D. Decomposition Behaviour of Mn(BH4)2 Formed by Ball-Milling $LiBH_4$ and $MnCl_2$. *J. Alloys Compd.* **2012**, *515*, 32−38.

(8) Paskevicius, M.; Ley, M. B.; Sheppard, D. A.; Jensen, T. R.; Buckley, C. E. Eutectic Melting in Metal Borohydrides. *Phys. Chem. Chem. Phys.* **2013**, *15*, 19774−19789.

(9) Černý, R.; Schouwink, P.; Sadikin, Y.; Stare, K.; Smrčok, L.; Richter, B.; Jensen, T. R. Trimetallic Borohydride $Li_3MZn_5(BH_4)_{15}$ (M = Mg, Mn) Containing Two Weakly Interconnected Frameworks. *Inorg. Chem.* **2013**, *52*, 9941−9947.

(10) Schouwink, P.; Ley, M. B.; Tissot, A.; Hagemann, H.; Jensen, T. R.; Smrčok, L.; Černý, R. Structure and Properties of Complex Hydride Perovskite Materials. *Nat. Commun.* **2014**, *5*, 5706.

(11) Filinchuk, Y.; Chernyshov, D.; Nevidomskyy, A.; Dmitriev, V. High-Pressure Polymorphism as a Step towards Destabilization of $LiBH_4$. *Angew. Chem., Int. Ed.* **2008**, *47*, 529−532.

(12) Nakano, S.; Nakayama, A.; Kikegawa, T. High-Pressure X-Ray Diffraction Study on Lithium Borohydride Using a Synchrotron Radiation. *J. Phys. Conf. Ser.* **2008**, *121*, 022021.

(13) Nakano, S.; Fujihisa, H.; Yamawaki, H.; Gotoh, Y.; Kikegawa, T. High-Pressure Transformations and Ionic Conductivity in Low-Z Complex Hydride $LiBH_4$. *Koatsuryoku no Kagaku to Gijutsu* **2011**, *21*, 213−220.

(14) Kim, E.; Kumar, R.; Weck, P. F.; Cornelius, A. L.; Nicol, M.; Vogel, S. C.; Zhang, J.; Hartl, M.; Stowe, A. C.; Daemen, L.; Zhao, Y. Pressure-Driven Phase Transitions in $NaBH_4$: Theory and Experiments. *J. Phys. Chem. B* **2007**, *111*, 13873−13876.

(15) Pistorius, C. W. F. T. Melting and Polymorphism of $LiBH_4$ to 45 Kbar. *Z. Phys. Chem.* **1974**, *88*, 253−263.

(16) Talyzin, A. V.; Andersson, O.; Sundqvist, B.; Kurnosov, A.; Dubrovinsky, L. High-Pressure Phase Transition in $LiBH_4$. *J. Solid State Chem.* **2007**, *180*, 510−517.

DOI: 10.1021/acs.chemmater.5b04102
Chem. Mater. 2016, 28, 274−283

(17) Kumar, R. S.; Kim, E.; Cornelius, A. L. Structural Phase Transitions in the Potential Hydrogen Storage Compound KBH_4 under Compression. *J. Phys. Chem. C* **2008**, *112*, 8452−8457.
(18) Filinchuk, Y.; Richter, B.; Jensen, T. R.; Dmitriev, V.; Chernyshov, D.; Hagemann, H. Porous and Dense Magnesium Borohydride Frameworks: Synthesis, Stability, and Reversible Absorption of Guest Species. *Angew. Chem., Int. Ed.* **2011**, *50*, 11162−11166.
(19) Kumar, R. S.; Cornelius, A. L. Structural Phase Transitions in $RbBH_4$ under Compression. *J. Alloys Compd.* **2009**, *476*, 5−8.
(20) Filinchuk, Y.; Talyzin, a.; Chernyshov, D.; Dmitriev, V. High-Pressure Phase of $NaBH_4$: Crystal Structure from Synchrotron Powder Diffraction Data. *Phys. Rev. B: Condens. Matter Mater. Phys.* **2007**, *76*, 092104.
(21) Ban, V.; Soloninin, A. V.; Skripov, A. V.; Hadermann, J.; Abakumov, A.; Filinchuk, Y. Pressure-Collapsed Amorphous $Mg(BH_4)_2$: An Ultradense Complex Hydride Showing a Reversible Transition to the Porous Framework. *J. Phys. Chem. C* **2014**, *118*, 23402−23408.
(22) Černý, R.; Penin, N.; Hagemann, H.; Filinchuk, Y. The First Crystallographic and Spectroscopic Characterization of a 3d-Metal Borohydride: $Mn(BH_4)_2$. *J. Phys. Chem. C* **2009**, *113*, 9003−9007.
(23) Tumanov, N.; Safin, D.; Richter, B.; Łodziana, Z.; Jensen, T. R.; Garcia, Y.; Filinchuk, Y. Challenges in the Synthetic Routes to $Mn(BH_4)_2$: Insight into Intermediate Compounds. *Dalt. Trans.* **2015**, *44*, 6571−6580.
(24) Allan, D. R.; Miletich, R.; Angel, R. J. A Diamond-Anvil Cell for Single-Crystal X-Ray Diffraction Studies to Pressures in Excess of 10 GPa. *Rev. Sci. Instrum.* **1996**, *67*, 840.
(25) Forman, R. A.; Piermarini, G. J.; Barnett, J. D.; Block, S. Pressure Measurement Made by the Utilization of Ruby Sharp-Line Luminescence. *Science* **1972**, *176*, 284−285.
(26) Piermarini, G. J.; Block, S.; Barnett, J. D.; Forman, R. A. Calibration of the Pressure Dependence of the R1 Ruby Fluorescence Line to 195 Kbar. *J. Appl. Phys.* **1975**, *46*, 2774.
(27) Piermarini, G. J. Hydrostatic Limits in Liquids and Solids to 100 Kbar. *J. Appl. Phys.* **1973**, *44*, 5377.
(28) Adams, D. M.; Appleby, R.; Sharma, S. K. Spectroscopy at Very High Pressures. X. Use of Ruby R-Lines in the Estimation of Pressure at Ambient and at Low Temperatures. *J. Phys. E: Sci. Instrum.* **1976**, *9*, 1140−1144.
(29) Hammersley, A. P.; Svensson, S. O.; Hanfland, M.; Fitch, A. N.; Hausermann, D. Two-Dimensional Detector Software: From Real Detector to Idealised Image or Two-Theta Scan. *High Pressure Res.* **1996**, *14*, 235−248.
(30) Dyadkin, V. *SNBL Tool Box*. Swiss Norwegian Beamline at ESRF: Grenoble, France, 2013.
(31) Vogel, S.; Ehm, L.; Knorr, K.; Braun, G. Automated Processing of 2D Powder Diffraction Data. *Adv. X-ray Anal.* **2002**, *45*, 31−33.
(32) Jensen, T. R.; Nielsen, T. K.; Filinchuk, Y.; Jørgensen, J.-E.; Cerenius, Y.; Gray, E. M.; Webb, C. J. Versatile in Situ Powder X-Ray Diffraction Cells for Solid-Gas Investigations. *J. Appl. Crystallogr.* **2010**, *43*, 1456−1463.
(33) Rodríguez-Carvajal, J. Recent Advances in Magnetic Structure Determination by Neutron Powder Diffraction. *Phys. B* **1993**, *192*, 55−69.
(34) Kraus, W.; Nolze, G. POWDER CELL; a Program for the Representation and Manipulation of Crystal Structures and Calculation of the Resulting X-Ray Powder Patterns. *J. Appl. Crystallogr.* **1996**, *29*, 301−303.
(35) Kresse, G.; Furthmüller, J. Efficiency of ab-initio Total Energy Calculations for Metals and Semiconductors Using a Plane-Wave Basis Set. *Comput. Mater. Sci.* **1996**, *6*, 15−20.
(36) Kresse, G.; Furthmüller, J. Efficient Iterative Schemes for ab initio Total-Energy Calculations Using a Plane-Wave Basis Set. *Phys. Rev. B: Condens. Matter Mater. Phys.* **1996**, *54*, 11169.
(37) Blöchl, P. E. Projector Augmented-Wave Method. *Phys. Rev. B: Condens. Matter Mater. Phys.* **1994**, *50*, 17953−17979.
(38) Perdew, J. P.; Burke, K.; Ernzerhof, M. Generalized Gradient Approximation Made Simple. *Phys. Rev. Lett.* **1996**, *77*, 3865−3868.
(39) Anisimov, V. I.; Zaanen, J.; Andersen, O. K. Band Theory and Mott Insulators: Hubbard U instead of Stoner I. *Phys. Rev. B: Condens. Matter Mater. Phys.* **1991**, *44*, 943−954.
(40) Franchini, C.; Podloucky, R.; Paier, J.; Marsman, M.; Kresse, G. Ground-State Properties of Multivalent Manganese Oxides: Density Functional and Hybrid Density Functional Calculations. *Phys. Rev. B: Condens. Matter Mater. Phys.* **2007**, *75*, 195128.
(41) Wang, L.; Maxisch, T.; Ceder, G. Oxidation Energies of Transition Metal Oxides within the GGA+U Framework. *Phys. Rev. B: Condens. Matter Mater. Phys.* **2006**, *73*, 195107.
(42) Togo, A.; Oba, F.; Tanaka, I. First-Principles Calculations of the Ferroelastic Transition between Rutile-Type and $CaCl_2$-Type SiO_2 at High Pressures. *Phys. Rev. B: Condens. Matter Mater. Phys.* **2008**, *78*, 134106.
(43) Nosé, S. A Unified Formulation of the Constant Temperature Molecular Dynamics Methods. *J. Chem. Phys.* **1984**, *81*, 511−519.
(44) Hoover, W. G. Canonical Dynamics: Equilibrium Phase-Space Distributions. *Phys. Rev. A: At., Mol., Opt. Phys.* **1985**, *31*, 1695−1697.
(45) Stokes, H. T.; Hatch, D. M. FINDSYM: Program for Identifying the Space-Group Symmetry of a Crystal. *J. Appl. Crystallogr.* **2005**, *38*, 237−238.
(46) Blanchard, D.; Zatti, M.; Vegge, T. Analysis of the Decomposition Gases from α and β-$Cd(BH_4)_2$ Synthesized by Temperature Controlled Mechanical Milling. *J. Alloys Compd.* **2013**, *547*, 76−80.
(47) Yao, Y.; Klug, D. D. High-Pressure Phases of Lithium Borohydride $LiBH_4$: A First-Principles Study. *Phys. Rev. B: Condens. Matter Mater. Phys.* **2012**, *86*, 064107.
(48) Zhou, X.-F.; Oganov, A. R.; Qian, G.-R.; Zhu, Q. First-Principles Determination of the Structure of Magnesium Borohydride. *Phys. Rev. Lett.* **2012**, *109*, 245503.
(49) Lindemann, I.; Ferrer, R. D.; Dunsch, L.; Černý, R.; Hagemann, H.; D'Anna, V.; Filinchuk, Y.; Schultz, L.; Gutfleisch, O. Novel Sodium Aluminium Borohydride Containing the Complex Anion $[Al(BH_4,Cl)_4]^-$. *Faraday Discuss.* **2011**, *151*, 231.
(50) Rude, L. H.; Filinchuk, Y.; Sørby, M. H.; Hauback, B. C.; Besenbacher, F.; Jensen, T. R. Anion Substitution in $Ca(BH_4)_2 - CaI_2$: Synthesis, Structure and Stability of Three New Compounds. *J. Phys. Chem. C* **2011**, *115*, 7768−7777.
(51) Rude, L. H.; Groppo, E.; Arnbjerg, L. M.; Ravnsbæk, D. B.; Malmkjær, R. A.; Filinchuk, Y.; Baricco, M.; Besenbacher, F.; Jensen, T. R. Iodide Substitution in Lithium Borohydride, $LiBH_4$−LiI. *J. Alloys Compd.* **2011**, *509*, 8299−8305.
(52) Rude, L. H.; Zavorotynska, O.; Arnbjerg, L. M.; Ravnsbæk, D. B.; Malmkjær, R. A.; Grove, H.; Hauback, B. C.; Baricco, M.; Filinchuk, Y.; Besenbacher, F.; Jensen, T. R. Bromide Substitution in Lithium Borohydride, $LiBH_4$−LiBr. *Int. J. Hydrogen Energy* **2011**, *36*, 15664−15672.
(53) Černý, R.; Ravnsbæk, D. B.; Schouwink, P.; Filinchuk, Y.; Penin, N.; Teyssier, J.; Smrčok, L.; Jensen, T. R. Potassium Zinc Borohydrides Containing Triangular $[Zn(BH_4)_3]^-$ and Tetrahedral $[Zn(BH_4)_xCl_{4-x}]^{2-}$ Anions. *J. Phys. Chem. C* **2012**, *116*, 1563−1571.
(54) Ravnsbæk, D. B.; Ley, M. B.; Lee, Y.-S.; Hagemann, H.; D'Anna, V.; Cho, Y. W.; Filinchuk, Y.; Jensen, T. R. A Mixed-Cation Mixed-Anion Borohydride $NaY(BH_4)_2Cl_2$. *Int. J. Hydrogen Energy* **2012**, *37*, 8428−8438.
(55) Ley, M. B.; Ravnsbæk, D. B.; Filinchuk, Y.; Lee, Y.-S.; Janot, R.; Cho, Y. W.; Skibsted, J.; Jensen, T. R. $LiCe(BH_4)_3Cl$, a New Lithium-Ion Conductor and Hydrogen Storage Material with Isolated Tetranuclear Anionic Clusters. *Chem. Mater.* **2012**, *24*, 1654−1663.
(56) Ley, M. B.; Boulineau, S.; Janot, R.; Filinchuk, Y.; Jensen, T. R. New Li Ion Conductors and Solid State Hydrogen Storage Materials: $LiM(BH_4)_3Cl$, M = La, Gd. *J. Phys. Chem. C* **2012**, *116*, 21267−21276.
(57) Ravnsbæk, D. B.; Nickels, E. A.; Černý, R.; Olesen, C. H.; David, W. I. F.; Edwards, P. P.; Filinchuk, Y.; Jensen, T. R. Novel Alkali Earth Borohydride $Sr(BH_4)_2$ and Borohydride-Chloride $Sr(BH_4)Cl$. *Inorg. Chem.* **2013**, *52*, 10877−10885.

DOI: 10.1021/acs.chemmater.5b04102
Chem. Mater. 2016, 28, 274−283

(58) Matsuo, M.; Takamura, H.; Maekawa, H.; Li, H.-W.; Orimo, S. Stabilization of Lithium Superionic Conduction Phase and Enhancement of Conductivity of $LiBH_4$ by LiCl Addition. *Appl. Phys. Lett.* **2009**, *94*, 084103.
(59) Maekawa, H.; Matsuo, M.; Takamura, H.; Ando, M.; Noda, Y.; Karahashi, T.; Orimo, S. Halide-Stabilized $LiBH_4$, a Room-Temperature Lithium Fast-Ion Conductor. *J. Am. Chem. Soc.* **2009**, *131*, 894−895.
(60) Mosegaard, L.; Moller, B.; Jorgensen, J.-E.; Filinchuk, Y.; Cerenius, Y.; Hanson, J. C.; Dimasi, E.; Besenbacher, F.; Jensen, T. R. Reactivity of $LiBH_4$: In Situ Synchrotron Radiation Powder X-Ray Diffraction Study. *J. Phys. Chem. C* **2008**, *112*, 1299−1303.
(61) Haridasan, T. M. The Raman Spectrum of Lithium Chloride. *Opt. Commun.* **1973**, *9*, 296−297.
(62) Filinchuk, Y.; Černý, R.; Hagemann, H. Insight into $Mg(BH_4)_2$ with Synchrotron X-Ray Diffraction: Structure Revision, Crystal Chemistry, and Anomalous Thermal Expansion. *Chem. Mater.* **2009**, *21*, 925−933.
(63) Roedern, E.; Jensen, T. R. Thermal Decomposition of $Mn(BH_4)_2$−$M(BH_4)X$ and $Mn(BH_4)_2$−MHX Composites with M = Li, Na, Mg, and Ca. *J. Phys. Chem. C* **2014**, *118*, 23567−23574.
(64) Mosegaard, L.; Møller, B.; Jørgensen, J.-E.; Bösenberg, U.; Dornheim, M.; Hanson, J. C.; Cerenius, Y.; Walker, G.; Jakobsen, H. J.; Besenbacher, F.; Jensen, T. R. Intermediate Phases Observed during Decomposition of $LiBH_4$. *J. Alloys Compd.* **2007**, *446*−*447*, 301−305.
(65) Züttel, A.; Rentsch, S.; Fischer, P.; Wenger, P.; Sudan, P.; Mauron, P.; Emmenegger, C. Hydrogen Storage Properties of $LiBH_4$. *J. Alloys Compd.* **2003**, *356*−*357*, 515−520.

DOI: 10.1021/acs.chemmater.5b04102
Chem. Mater. 2016, 28, 274−283